

FLOW STRUCTURE AND MIXING MECHANISM IN AN AGITATED THIN-FILM EVAPORATOR

SATORU KOMORI, KAZUTAKA TAKATA AND YASUHIRO MURAKAMI

Department of Chemical Engineering, Kyushu University, Fukuoka 812

Key Words: Fluid Mechanics, Agitation, Evaporator, Thin-Film Flow, Mixing

The flow structure and mixing mechanism of the high-viscosity fluid in an agitated thin-film evaporator were experimentally and numerically investigated. Film thickness, holdup and power consumption were measured, and velocity distributions were numerically calculated using a finite element method. The results show that most of the fluid flows down in a fillet and that mixing between fillet and film is extremely suppressed. This also suggests that usual thin-film evaporators are not always effective.

Introduction

Agitated thin-film evaporators are widely used to concentrate polymer solutions by evaporating solvents in industrial processes. The evaporator can be operated in a vacuum, and the residence time of a solution in the equipment can be reduced to less than a few seconds. The agitated thin-film evaporator can therefore find wide application in food, pharmaceutical and petrochemical processes which involve the operations of refining, concentration or deodorization. In such processes the solutions are often prone to thermal decomposition, or have the high viscosity or low thermal conductivity, making the thin-film evaporator even more useful. The evaporator equipment and its application are described in detail by Leonald³⁾ and Mutzenburg *et al.*⁵⁾

An agitated thin-film evaporator with a rotor blade is sketched in Fig. 1. The supplied fluid flows down along the vertical cylindrical shell-wall and is agitated by a rotor blade. A clearance is held as a gap between the fixed blade-tip and the cylindrical wall. The agitation by the blade forms a film falling along the cylindrical wall and a falling fillet in the periphery of the blade. The falling film consists of both a radial drag flow due to the rotor blade and a downward flow due to gravity. The fillet consists of a falling spiral flow. These flow configurations suggest that the film flow may contribute both to heat transfer between the

fluid and the cylindrical wall and evaporation through the film surface, and that the fillet flow may predominate in momentum and mass transfer between the film and the fillet. Thus, it is of great importance to investigate the flow structure and mixing mechanism in the film and fillet flows in designing an effective thin-film evaporator.

Kern and Karakas²⁾ and Godau¹⁾ analytically calculated the film thickness and falling velocity of high-viscosity fluid in the thin-film evaporator under isothermal conditions without evaporation. Their analyses were based on the equations of motion. However, they neither compared the predictions with the measurements nor analyzed the flow structure in the fillet. Nakamura and Watanabe⁶⁾ investigated the low-viscosity flow in an agitated thin-film evaporator under isothermal operating conditions. They approximately estimated the fillet size on the (r, θ) -plane and calculated the liquid holdup by means of a

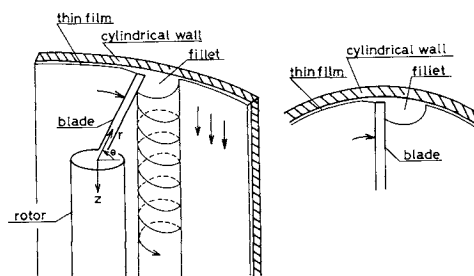


Fig. 1. Schematic diagram of an agitated thin-film evaporator and flow field

hydraulic jump theory. Finally, they showed that the predictions were in good agreement with the measurements. McKelvey and Sharps⁴) calculated the mass balance on the (r, θ) -plane of an isothermal high-viscosity flow by using the measurement of the film thickness and then estimated the size of the fillet. The predictions also showed the good agreement with the measurements. However, the calculations of Nakamura and Watanabe⁶) and McKelvey and Sharps⁴) were not faithfully based on the equations of motion, and so they could not give the details of the flow structure and mixing mechanism which are most useful for the optimum design of an evaporator.

The purpose of the present work was to investigate experimentally and numerically the flow structure and mixing mechanism in an agitated thin-film evaporator with high-viscosity fluid and to examine whether the usual evaporators are really effective or not. Both experiments and calculations were conducted under isothermal conditions without evaporation (as well as under conditions reported in the published works). This is because the flow structure and mixing mechanism under isothermal flow conditions without evaporation are similar to those under non-isothermal conditions with evaporation, since both the fillet and film are also formed in an apparatus under the flow condition with evaporation. Power consumption, film thickness and holdup were measured. The Navier-Stokes equations were numerically solved using a finite-element method to obtain details of the flow structure and mixing mechanism, and the momentum and mass transfer between the film and fillet were studied by means of a Lagrangian random-walk model.

1. Experiments

Figure 2 shows a schematic diagram of the experimental apparatus and measuring system. The experiments were conducted under isothermal conditions without evaporation. The model apparatus of an agitated thin-film evaporator used here was made of a stainless steel cylinder of 0.25 m inner diameter, 0.5 m length and 50 μm out-of-roundness, and it incorporated a scraper-blade. The blade was made of a 0.003 m-thick stainless-steel plate and was 0.15 m long. The clearance between the blade-tip and the cylindrical wall was adjusted by changing the radial length of the blade. The clearance was measured using an eddy current-type non-contact gap-detector (GAP SENSOR PU-05, Applied Electronics Co., Ltd.) mounted on the cylinder. The Newtonian high-viscosity fluid used was a corn syrup and it was fed from the top of the cylinder vessel by a gear pump at a constant flow-rate. The fluid falling along the cylinder wall was agitated by the blade, and a film and a fillet were formed as shown in Fig. 1.

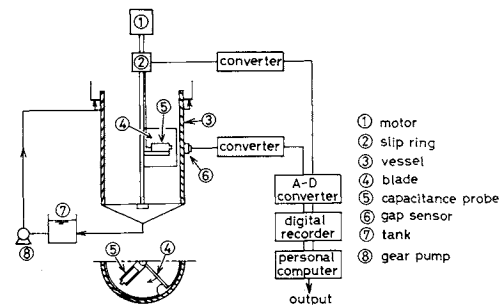


Fig. 2. Experimental apparatus and measuring system

Table 1. Experimental conditions

	Power consumption	Film thickness	Holdup
μ [Pa·s]	1.02–13.42	1.36– 5.76	2.10–6.65
Γ [$\text{kg} \cdot \text{m}^{-1} \cdot \text{s}^{-1}$]	0.01– 0.03	0.01– 0.03	0.01–0.03
h_0 [mm]	0.58– 1.69	1.1 – 1.5	1.0
u_b [$\text{m} \cdot \text{s}^{-1}$]	5.24–10.48	5.24–10.48	5.24–9.17

The film thickness was measured using an electrostatic-type non-contact gap-detector (DT-231, IWATSU Co., Ltd.). A capacitance probe was mounted on the shaft and was rotated with the blade. The output signal from the capacitance probe was transmitted to an A/D converter through a slip ring. The film thickness was determined by subtracting the measured distance between the probe surface and the thin-film surface from the distance between the probe surface and the cylindrical wall surface.

The power consumption was measured using a strain gage-type torque-transducer (TP-1KMAF KYOWA Electric Industry Co., Ltd.) attached to the shaft. The torque was obtained by subtracting the no-load torque from the total torque (the reading of the meter).

The holdup defined by the fluid mass being held in the equipment was measured by simultaneously shutting off the flow at the top and bottom of the vessel.

The signals from the instruments above were transmitted to a digital recorder through an A/D converter and processed by a personal computer.

The experimental conditions are listed in Table 1.

2. Numerical Calculations

It is of great importance to measure the fluid velocities in the fillet in clarifying the flow structure and mixing mechanism in an agitated thin-film evaporator. The measurement is, however, an extremely difficult task, because neither hot-film nor laser-Doppler velocimeter is applicable to the complicated recirculating flow with the curved free surface. In such case, numerical calculations often become a useful tool for determining velocity distributions. Thus, numerical calculations of velocity distributions were

adopted in this study.

The governing equations of an incompressible, steady fluid flow in a fillet are given by

$$\frac{\partial^2 \psi}{\partial x^2} + \frac{\partial^2 \psi}{\partial y^2} = -\omega \quad (1)$$

$$\frac{\partial \omega}{\partial t} + \frac{\partial \psi}{\partial y} \frac{\partial \omega}{\partial x} - \frac{\partial \psi}{\partial x} \frac{\partial \omega}{\partial y} = v \left(\frac{\partial^2 \omega}{\partial x^2} + \frac{\partial^2 \omega}{\partial y^2} \right) \quad (2)$$

$$\frac{\partial w}{\partial t} + u \frac{\partial w}{\partial x} + v \frac{\partial w}{\partial y} = v \left(\frac{\partial^2 w}{\partial x^2} + \frac{\partial^2 w}{\partial y^2} \right) + g \quad (3)$$

$$\omega = \frac{\partial v}{\partial x} - \frac{\partial u}{\partial y} \quad (4)$$

$$u = \frac{\partial \psi}{\partial y} \quad (5)$$

$$v = -\frac{\partial \psi}{\partial x} \quad (6)$$

Here the derivatives of the velocities and pressure with respect to the axial coordinate z are neglected. This means that the shape of the fillet does not change in the axial direction. Further, the flow field of the fillet on the horizontal (r, θ) -plane was approximated by the rectangular coordinates, x and y , as shown in **Fig. 4**. This approximation is based on the fact that the curvature of the cylindrical vessel (250 mm) is so large compared to the radial and tangential sizes of the fillet (about 7–8 mm and 15 mm). Equations (1) and (2) were solved using a Galerkin finite-element method combined with FTCS (forward-time centered-space) scheme. A flow chart of the numerical scheme is shown in **Fig. 3**. The convergence criterion at each point of the mesh was

$$\left| \frac{\omega^{n+1} - \omega^n}{\omega^n} \right| < \varepsilon = 0.001 \quad (7)$$

where the superscript n shows the number of numerical iterations. In this study, the stationary solutions of ψ and ω were given by the quasi-steady solutions of Eqs. (1) and (2) satisfying the convergence criterion. The axial velocity w was computed by substituting the velocities, u and v , obtained by solving Eqs. (1) and (2) into Eq. (3).

Boundary conditions for the numerical calculations are given in **Fig. 4**. In this study, the experiments were conducted by moving the blade, but the numerical calculations were examined by moving the cylindrical wall and fixing the blade as shown in the **Fig. 4**. This is because the moving-wall system can simplify the calculations and because it can more clearly describe the fluid motion in the fillet. The shape and position of the free surface were approximately given by experimental photographs, and those of the meniscus behind the blade were approximated by a circular arc. The wall-boundary value of the vorticity was given by

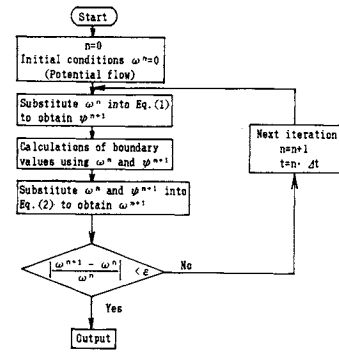


Fig. 3. Flow chart of the numerical scheme

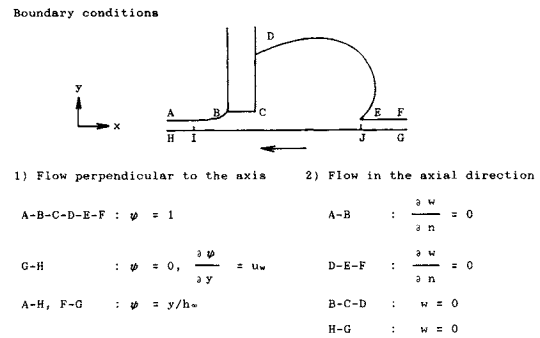


Fig. 4. Boundary conditions for numerical calculations

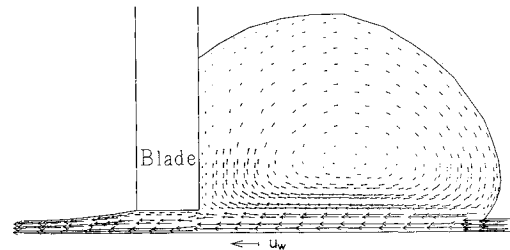


Fig. 5. Predicted velocity vectors in the fillet; $u_w = 5.24 \text{ m} \cdot \text{s}^{-1}$; $h_0 = 0.001 \text{ m}$; $Re_L = 0.03$

the method of Woods.⁷⁾

3. Results and Discussion

3.1 Flow structure

Figure 5 shows the predicted velocity vectors (u, v) on the (x, y) -plane. The flow direction is reversed in front of the blade, and a circulating flow is formed in the fillet. The velocity inside the fillet is faster than that near the free surface, and in the central region the velocity is small. The flow pattern can be more clearly observed in the distributions of the contours of the stream function (**Fig. 6**). Almost all the streamlines which stretch from the film to the fillet are parallel to the wall and come into the clearance between the blade-tip and the wall. This suggests that the fluid intruding from the film into the fillet region shortly passes the clearance without being mixed with the circulating fluid.

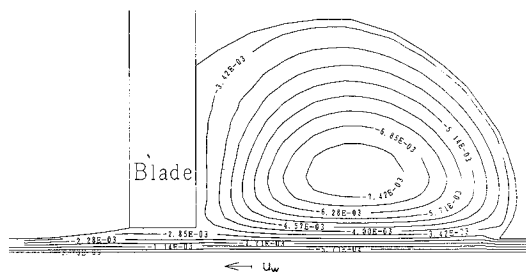


Fig. 6. Contours of predicted streamlines in the fillet. Numbers in the figure show values of the stream function; $u_w = 5.24 \text{ m} \cdot \text{s}^{-1}$; $h_0 = 0.001 \text{ m}$; $Re_L = 0.03$

The measured values of power consumption in one blade are shown in **Fig. 7**. It is found that the power consumption is well correlated with the curve shown by a solid line within $\pm 30\%$ deviation:

$$N_P = 6.02 \cdot Re_M^{-6/5} \cdot Re_L^{3/10} \cdot (h_0/d)^{-4/5} \quad (8)$$

where Re_M is the mixing Reynolds number, Re_L the film Reynolds number and h_0/d the dimensionless clearance. The power of Re_M is 20% smaller than that of the -1 value obtained in a laminar stirred-vessel flow. In addition to the above measurements, P_w was numerically calculated by

$$P_{w, \text{cal}} = u_w \cdot L_b \cdot \mu \cdot \int \frac{du}{dy} dl \quad (9)$$

where L_b is the axial length of the blade, u_w the wall velocity (the relative velocity between the blade and the cylindrical wall) and μ the viscosity. Here the first derivative of u was integrated over the cylindrical wall between two points I and J shown in **Fig. 4**. The predictions shown by a dotted line in **Fig. 7** are in good agreement with the measurements. This validates the present numerical calculations.

Figure 8 shows the contours of the axial velocity w predicted by Eq. (3). The axial velocity increases with increasing distance from the wall boundaries of the blade and the cylindrical wall, and the maximum velocity appears in the free-surface region of the top of the fillet. Prediction of the axial velocity can be justified by estimating the flow-rate in the fillet and film. When the total flow-rate in the equipment is denoted by Q , the flow-rates in the fillet and film, Q_f and Q_m , are given by the mass-balance equation

$$Q = Q_m + Q_f \quad (10)$$

Here, Q_f and Q_m are defined by

$$Q_m = \pi \cdot d \cdot h_\infty \cdot \bar{w}_m \quad (11)$$

$$Q_f = \pi \cdot d \cdot (\bar{h} - h_\infty) \cdot \bar{w}_f \quad (12)$$

where h_∞ is the film thickness, \bar{h} the apparent film thickness obtained by averaging the total flow-rate over the cylindrical-vessel surface, d the inner diameter of the cylindrical vessel, \bar{w}_m the cross-sectional

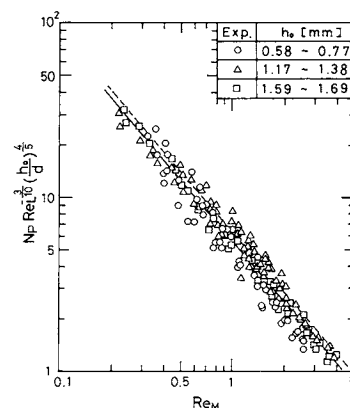


Fig. 7. Comparison between measured and predicted power consumption

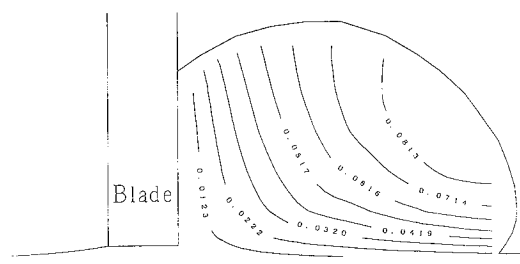


Fig. 8. Contours of predicted axial velocity in the fillet. Numbers in the figure show values of the axial velocity w [$\text{m} \cdot \text{s}^{-1}$]; $u_w = 5.24 \text{ m} \cdot \text{s}^{-1}$; $h_0 = 0.001 \text{ m}$; $Re_L = 0.03$

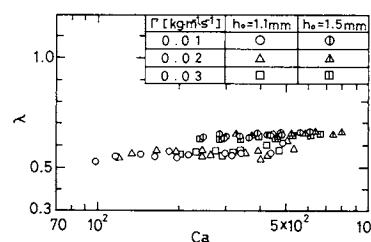


Fig. 9. Dependence of capillary number on dimensionless film thickness

mean velocity of the film in the axial direction, and \bar{w}_f denotes the cross-sectional mean velocity of the fillet. An unknown variable in Eqs. (10)–(12) is \bar{w}_f , which should be determined from measurements of h_∞ and \bar{h} . The measured values of the dimensionless film thickness, $\lambda (= h_\infty/h_0)$, are shown against the capillary number, Ca , in **Fig. 9**. The dimensionless film thickness λ does not depend on Ca , but does depends on the clearance h_0 . The values of λ also show that the film thickness h_∞ is 55–65% of the clearance h_0 . The average film thickness \bar{h} was estimated by

$$\bar{h} = H_0 / (\rho \cdot \pi \cdot d \cdot L_b) \quad (13)$$

Here, H_0 is the holdup in the region with the blade. The film flow in the blade region was experimentally confirmed to be close to a laminar falling film so that \bar{w}_m was calculated by use of both the Nusselt equation

and the measured value of h_{∞} . When these values of h_{∞} , \bar{h} , and \bar{w}_m are substituted into Eqs. (10)–(12), \bar{w}_f can be obtained.

Figure 10 shows the values of \bar{w}_f and \bar{w}_m against the film Reynolds number Re_L . The predictions shown by the dotted line in **Fig. 10** are in good agreement with the measurements. It is also found that \bar{w}_f and \bar{w}_m are well correlated by Re_L :

$$\bar{w}_f = 0.33 \cdot Re_L^{1/2} \quad (14)$$

$$\bar{w}_m = 0.0165 \cdot Re_L^{1/2} \quad (15)$$

The correlations show that the cross-sectional mean velocity of the fillet is 20 times that of the film. This suggests that most of the fluid flows down in the fillet. This also becomes clear by plotting the ratio of the flow-rate in the fillet, Q_f , to the total flow-rate, Q , as shown in **Fig. 11**. Here the ratio of the flow-rate in the fillet, Q_f , to the total flow-rate, Q , was calculated by:

$$Q_f/Q = (Q - Q_m)/Q \quad (16)$$

The ratio shows that 70–90% of the total flow-rate flows down in the fillet.

3.2 Mixing mechanism

As the most of the fluid flows down in the fillet, the exchange rate of the fluid between fillet and film may be reduced. To investigate the exchange rate, the Lagrangian random-walk model of Sawford and Hunt⁸⁾ was used together with numerical calculations of the velocity field. The model assumed that marked particles in the flow field are moved by the combined actions of the advective velocity and molecular diffusion. Then the particle displacements in the x - and y -directions are given by

$$dx = u \cdot dt + \sqrt{D} \cdot dW_d \quad (17)$$

$$dy = v \cdot dt + \sqrt{D} \cdot dW_d \quad (18)$$

where D is the molecular diffusivity of the mass and dW_d denotes the Gaussian white noise process with zero mean value and variance dt . The trajectories of the marked particles can be calculated by substituting u and v obtained from Eqs. (1)–(2) into Eqs. (17) and (18) and generating Gaussian random variables by a computer. **Figure 12** shows the trajectories of the marked particles intruding from the film into the fillet. The trajectories clearly show that all of the fluid intruding from the film region pass the clearance without being mixed with the circulating fluid in the fillet. This also means that most of the fluid in an actual evaporator flows down in the fillet without being effectively evaporated in the film and that the usual type of evaporator is not effective. Therefore, a new type which can promote the fluid exchange between the fillet and film should be developed.

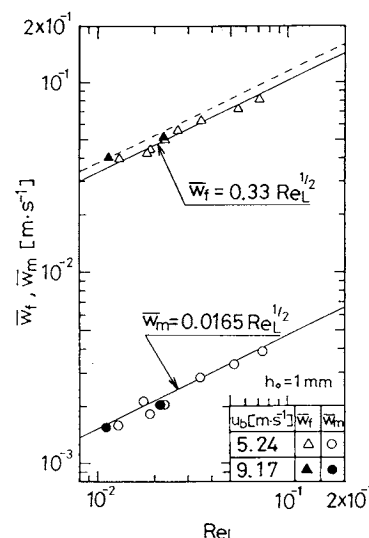


Fig. 10. Comparison between measured and predicted \bar{w}_f and \bar{w}_m [m·s⁻¹]

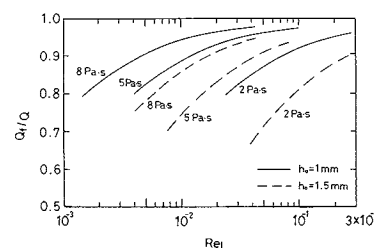


Fig. 11. Ratio of flow-rate in the fillet to total flow-rate

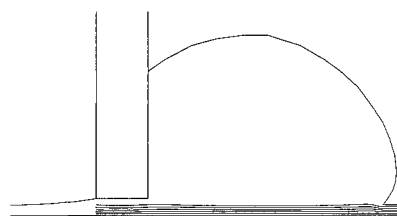


Fig. 12. Trajectories of marked particles in the fillet

Conclusions

The flow structure and mixing mechanism of high-viscosity fluid in an agitated thin-film evaporator were experimentally and numerically investigated under isothermal conditions without evaporation. The main results of this study can be summarized as follows.

(1) The laminar flow in an evaporator is divided into a fillet flow and a film flow. The fillet flow consists of a spiral motion, and fluid accounting for 70–90% of the total flow-rate flows down in the fillet. The film flow can be considered to be a laminar falling film flow along the cylindrical wall, and its falling velocity and flow-rate are very small compared to those of the fillet.

(2) Mixing of the fluid between the fillet and film is extremely suppressed. This reduces the efficiency of

the thin-film evaporator.

These results indicate that the usual evaporators are not always effective, and that they should be improved to promote the fluid mixing between fillet and film.

Acknowledgment

The authors would like to thank Dr. M. Takao, Messrs. I. Hirose and K. Kawamura for their help in conducting the experiments.

Nomenclature

C_a	= capillary number, $C_a = \mu \cdot u_w / \sigma$	[—]
d	= inner diameter of the cylindrical vessel	[m]
H_0	= holdup in the region with the blade	[kg]
h_0	= clearance between blade-tip and cylindrical wall	[m]
h_∞	= film thickness	[m]
\bar{h}	= averaged film thickness	[m]
L_b	= axial blade length	[m]
n	= rotation number	[s ⁻¹]
N_p	= power number, $N_p = P_w / (\rho \cdot (n \cdot d)^3 \cdot h_0 \cdot L_b)$	[—]
P_w	= power consumption	[J · s ⁻¹]
$P_{w,cal}$	= calculated power consumption	[J · s ⁻¹]
Q	= total mass flow-rate	[m ³ · s ⁻¹]
Q_f	= mass flow-rate in the fillet	[m ³ · s ⁻¹]
Q_m	= mass flow-rate in the film	[m ³ · s ⁻¹]
Re_L	= film Reynolds number, $Re_L = 4\Gamma / \mu$	[—]
Re_M	= mixing Reynolds number, $Re_M = \rho \cdot n \cdot d \cdot h_0 / \mu$	[—]
t	= time	[s]
u	= velocity component in the x direction	[m · s ⁻¹]
u_w	= velocity of a moving wall	[m · s ⁻¹]

v	= velocity component in the y direction	[m · s ⁻¹]
w	= velocity component in the z direction	[m · s ⁻¹]
\bar{w}_f	= downward axial velocity in the fillet	[m · s ⁻¹]
\bar{w}_m	= downward axial velocity in the film	[m · s ⁻¹]
Γ	= flow-rate per unit length	[kg · m ⁻¹ · s ⁻¹]
λ	= dimensionless film thickness, $\lambda = h_\infty / h_0$	[—]
μ	= viscosity	[Pa · s]
ν	= kinematic viscosity	[m ² · s ⁻¹]
ρ	= density	[kg · m ⁻³]
σ	= surface tension	[N · m ⁻¹]
ψ	= stream function	[m ² · s ⁻¹]
ω	= vorticity	[s ⁻¹]

<Superscript>

n = n -th iteration

Literature Cited

- Godau, H. G.: *Int. Chem. Eng.*, **15**, 445 (1975).
- Kern, D. Q. and H. G. Karakas: *Chem. Eng. Progr.*, **55**, 141 (1959).
- Leonald, E. N.: *Ind. Eng. Chem.*, **56**, 26 (1965).
- Mckelvey, J. M. and G. V. Sharps, Jr.: *Poly. Eng. Sci.*, **19**, 651 (1979).
- Mutzenburg, A. B., N. Paker and R. Fischer: *Chem. Eng.*, Sep. 13, 175 (1965).
- Nakamura, K. and T. Watanabe: *Chem. Eng. Commun.*, **18**, 173 (1982).
- Roache, P. J.: *Computational Fluid Dynamics*, Hermora Publishers (1976), p. 142.
- Sawford, B. L. and J. C. R. Hunt: *J. Fluid Mech.*, **165**, 373 (1986).